High-order curvilinear mesh generation from third-party meshes

Kaloyan S Kirilov* Joaquim Peiró† Jingtian Zhou‡ Mashy D Green§
David Moxey¶

Abstract

Established *a posteriori* mesh curving techniques often rely on an accurate CAD parametrisation of the underlying mesh objects which may not always be available. To deal with such cases, we propose a method for reconstructing the missing information between the mesh and the CAD geometry when importing an arbitrarily sourced straight-sided mesh. The reconstruction is followed by curving methods for order elevation, projections and, subsequently, optimisation. Lastly, mesh modification techniques are used to achieve the desired mesh resolution and quality. We illustrate the steps of the proposed workflow through a simple geometry and a complex automotive geometry.

1 Introduction

High-order high-fidelity solvers, such as Nektar++ [16], Nek5000 [7] or PyFR [26], require valid high-quality curvilinear meshes that accurately conform to the underlying geometry. Such meshes are commonly generated using *a posteriori* approach whereby a linear straight-sided mesh is generated first and then transformed into a straight-sided mesh of the required order. The edges and faces of this high-order mesh are then curved to lie on the curves and surfaces, respectively, which define the CAD geometry. Additional untangling and optimisation techniques are usually adopted during or after the curving to ensure validity and enhance the quality of the mesh [25, 22, 20]. Implementations of this approach are available in open-source tools such as Gmsh [9] and NekMesh [25], and in commercial codes such as GridPro and Pointwise (now Fidelity CFD) [12].

In an industrial setting, where geometries can consist of thousands of CAD surfaces and meshes, the development of a methodology capable to automatically, accurately and efficiently resolve the required flow features in fast turn-around time, presents a huge challenge for mesh generation tools. A natural solution is to take advantage of existing fast, robust and flexible mesh generators for linear meshes suited to industrial application. The main drawback of this approach is that some of these mesh generators do not provide the connectivity between the surface mesh and the underlying CAD objects and sometimes do not guarantee CAD compliance to increase robustness. This is of particular importance in the mesh curving process since most CAD related operations are usually performed in the parametric space of the CAD objects. If this information is available, one can elevate the order and curve to the corresponding CAD. One example is the work by Ruiz-Gironés et al. on the High-Lift Common Research model using Pointwise CAD API and extensive CAD cleaning [19] . Another example is the successful mesh generation, after a very extensive defeaturing and BRep simplification, and flow simulation of a full road sport car by the NekMesh team [15]. However, integration of *a posteriori* approaches in industry is hampered by the need of extensive and time-consuming CAD cleaning, the lack of CAD-mesh connectivity, and the lack of optimized projection procedures.

To make a step forward in tackling the previously mentioned problems, in this work, we present a generic methodology for generating high-order meshes from a very coarse linear mesh through the reconstruction of the missing mesh-CAD connectivity. Moreover, we ensure full CAD-conformity through vertex projections. This allows us to generate valid high-order meshes even from invalid, non-watertight CAD BRep STEPs of complex geometries, providing a valid watertight triangulation such as an STL is available. As this is assumed to be a solved challenge in the finite-volume community, this relaxes the requirements and the need for CAD simplification. With this newly acquired CAD-mesh information, we reuse and improve the internal bottom-up approaches for both mesh curving, isoparametric prism layer splitting, mesh optimisations and untangling as defined in [25] , [10].

The outline of this work is structured as follows. Section 2 presents a high-level overview of the methodology we propose for high-order mesh generation from third-party meshes and some key concepts as CAD conformity and CAD compliance. Section 3 discusses the

*Imperial College London.
†Imperial College London.
‡Imperial College London.
§Kings College London.
¶Kings College London.

implementation details, describing every module of the workflow, while focusing on the challenges and the proposed solutions that allow us to curve and optimise imported third-party linear meshes. Section 4 illustrates the methodology with two examples. The consistency of the workflow is verified first using a simple analytical geometry, a semi-sphere. The second example applies the procedure to a complex automotive geometry. We conclude this work with a short-term outline for the goals of developing further the workflow.

2 Overview of the Methodology

To tackle the problem of industrialisation of high-order methods for CFD applications, we propose a workflow capable of combining robust linear mesh generation tools with *a posteriori* mesh curving and optimisation. The starting point is a coarse straight-sided (linear) volume mesh with a prism layer that requires minimal CAD preparation for complex geometries. From that point the workflow will create a valid high-order mesh from any boundary-conforming linear mesh without relying on application-specific tools which exist, such as the PADRAM [2] or TAU meshers [8].

When generating the curvilinear mesh, we aim at reusing and, when possible, improving current high-order *a posteriori* curving and optimisation methodologies. However, these methods often rely on some critical assumptions that are not necessarily satisfied when using a third-party linear mesh:

- *CAD-conformity*: The vertices of the linear mesh lie on the CAD curves and surfaces within machine precision (ϵ_M).
- *CAD-connectivity*: The mesh curving and optimisation procedures require accurate information about the corresponding BRep object.
- *CAD-compliance*: The mesh curving processes may assume that every mesh face corresponds to precisely one BRep surface, which is not always the case for third-party meshes.

We propose a new intermediate step in the mesh generation process (see Figure 1) which first associates the vertices of the linear mesh with the closest BRep objects (Surface, Edge or Vertex) and their coordinates in parametric space. CAD conformity of the linear mesh is then ensured through vertex projection. We use a sophisticated series of logical steps to reconstruct the CAD connectivity of all surface entities of the mesh - edges and faces - associating each mesh objects with their corresponding BRep ones. With this link established, accurate parametric projections and surface optimisations are performed for mesh curving. To ensure validity and to increase the mesh quality, we can employ a variational optimiser to attempt untangling any invalid elements. An added advantage of the newly acquired CAD connectivity comes to the fore precisely with these optimisations, which allow a certain degree of sliding of the high-order nodes on the CAD BRep object.

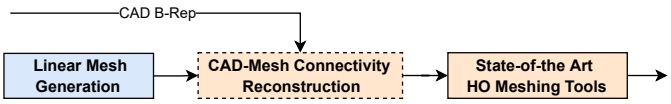

Figure 1: The proposed mesh generation workflow starts from third-party linear meshes (blue) which are processed by in house *a posteriori* high-order modules (orange).

A special consideration is taken when a linear element (boundary face or edge) crosses two BRep surfaces. In these rare cases, no BRep object is assigned to the mesh entity and is followed by a simplified projection process with no further optimisations. This might result in slight deterioration of the surface quality in cases where the multi-patch BRep has only C_0 continuity between patches. However, it also allows for significant flexibility on the linear mesh generation side, decreasing the need for CAD defeaturing and also facilitating the use of two separate geometrical representations for the linear mesh generation (e.g. a STL triangulation) and for the high-order part of the process (invalid STEP). How to achieve the right balance between surface quality and volume mesh generation flexibility will depend on the application and complexity of the case.

Lastly, the CAD reconstruction process is extended to high-order meshes which has two main advantages. Firstly, it provides the means for a mesh quality suite, where the geometrical accuracy of any high-order mesh can be evaluated, provided a CAD file is present. Secondly it permits the user to start the workflow from any third-party mesh, even a high-order curved one, assess its quality and then use in house optimisation techniques to improve its quality.

3 Proposed Workflow Implementation

This work employs, improves and further develops the modules and architecture of the high-order mesh generator NekMesh [10], that has been designed for the generation of unstructured highly-stretched hybrid meshes combining prismatic and tetrahedral elements, required for high-speed viscous flow simulations.

This section presents the proposed workflow, and discusses all stages of mesh generation, from CAD

preparation and linear mesh generation to final untangling. Particular interest will be paid to achieving the required resolution in the normal direction of the prism layers to accurately model the flow in the boundary layer. Figure 2 shows the main processes part of the workflow.

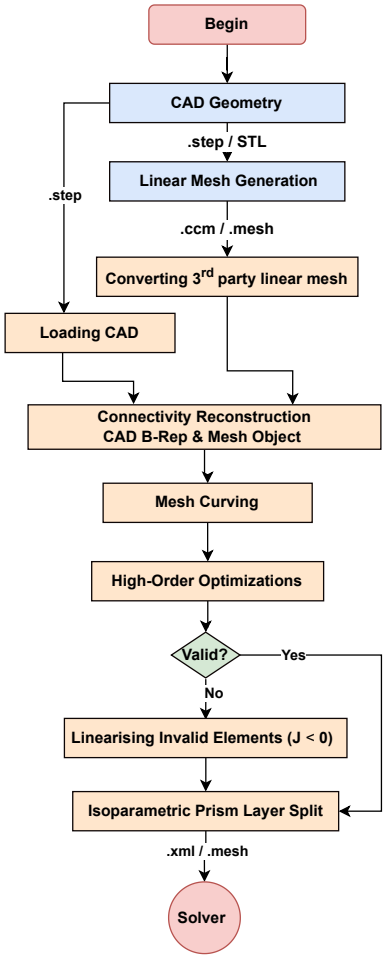

Figure 2: Overview of the end-to-end mesh generation pipeline, showing all steps/modules in generating the valid high-order mesh. Processes marked in blue are third-party software, whereas all orange ones are internal to NekMesh.

3.1 Linear Mesh Generation The starting point of the process is the creation of the underlying CAD model and the generation of the linear straight-sided mesh. The way these are generated is left completely to the desires and needs of the user. However, there are several notes and best practices that have been discovered during the development and the applications of this work. In terms of the CAD BRep, there are no specific requirements on the user for the generation. The only necessity on the high-order side of the process is the availability of a BRep in the form of a STEP file.

The workflow allows the generation of a linear mesh from various CAD file formats or even from a triangulation. This is advantadgeous when handling complex geometries because the B-Rep does not need to be watertight, and could have imperfections such as free edges, pierced surfaces, etc. Their presence leads to a slight deterioration of the surface quality of the mesh, but undertaking CAD repair could lead to unacceptable time scales in an industrial setting.

Currently, NekMesh supports the input from the following mesh generators: Gmsh (.msh), original Nektar (.plt) and StarCCM+ through the CCM to OpenFoam API [1]. Supporting other input formats is a relatively easy task due to the modularity of NekMesh [16].

3.2 Importance of Ensuring CAD Conformity and CAD Compliance In regions of high curvature, it is often observed that the mesh vertices do not lie precisely on the CAD. In the following we will denoted the minimum distance between a point and the target CAD object as δ. Such deviation is mainly due to inaccuracies of the mesh or to the CAD projection algorithm.

These geometrical errors significantly impact the geometrical accuracy of the mesh and, potentially, of the simulation. For instance, they could introduce waviness on the boundary of the mesh and trigger oscillatory behaviour in the solution. They can worsen discontinuities of tangents and normals at the interfaces between elements. Inaccurate projection during mesh curving leads to similar behaviour as illustrated in Figure 3.

Figure 3: Schematic showing an exaggerated effect of the geometry oscillations in a very coarse curved edge.

Figure 4 shows an example where a seemingly "very fine" tessellation unexpectedly generates a high deviation of $\delta \approx 2 \times 10^{-4}$ on the low curvature regions of a wing. A naive projection of the high-order nodes onto the BRep results in an unacceptable spike-like pattern on the curved surface mesh, which subsequently decreases the overall volume mesh quality.

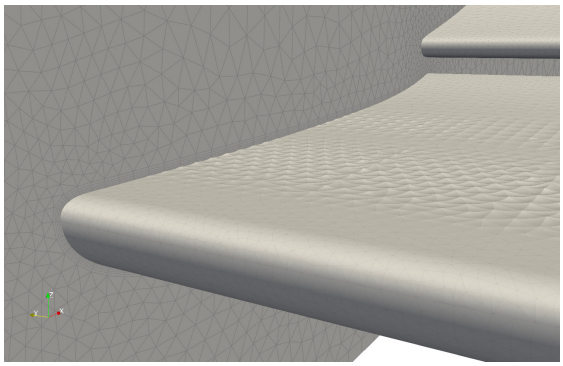

Figure 4: An illustration of the impact of the tessellation effect. A "very fine" surface mesh unexpectedly generates an oscillatory pattern on the regions of low curvature in a wing.

Multi-NURBS surfaces Watertight and valid complex CAD BRep often exhibit small and very skewed surfaces due to certain CAD operations such as fillets, see Figure 5. If the linear mesh is assumed to be CAD conformal in such instances, the generated mesh could have numerous highly skewed surfaces which will deteriorate volume mesh quality. A remedy employed by some linear meshers is to combine these troublesome CAD surfaces into multi-patch virtual geometries, but this could lead to inaccurate projections and self-intersections, see Figure 6, during the mesh curving stage.

Observation 1: The CAD conformity of the linear mesh is of crucial importance for the surface and volume mesh quality of the high-order mesh. Therefore, one must ensure appropriate treatment for the linear vertices on the high-order side of the process.

Observation 2: In the presence of multi-patch surfaces, a suitable linear mesh requires CAD compliance and minimising multi-patch element faces while keeping reasonable mesh quality. These conflicting requirements must be carefully accounted for through the linear meshing process or the use of mesh modification techniques *a posteriori* in NekMesh.

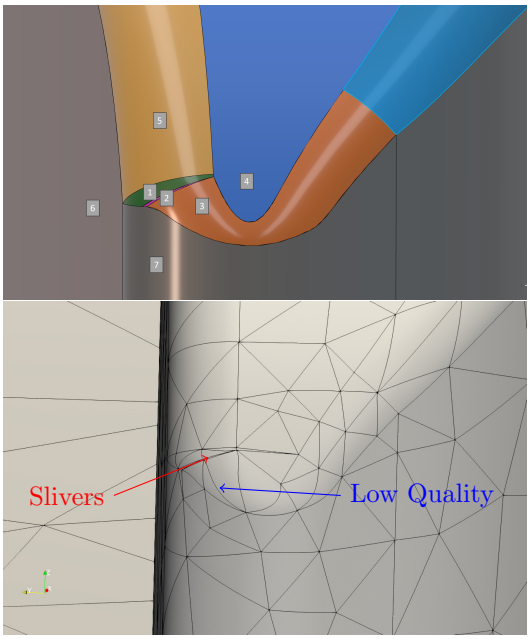

Figure 5: Area with 7 highly skewed CAD surfaces leading to sliver elements if CAD compliance is strictly enforced. Note the deterioration in mesh quality in elements if projections are inaccurate (blue).

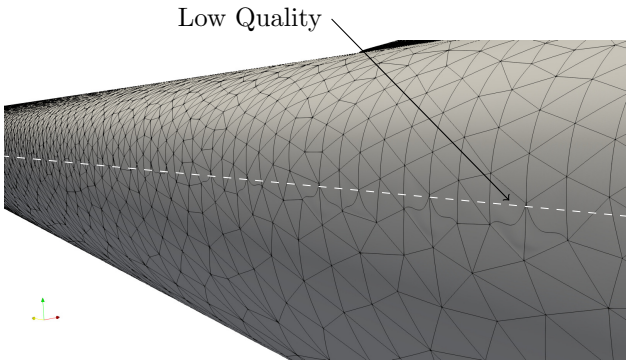

Figure 6: Mesh distortions due to naive projection on multi-patch elements (BRep line in white) at polynomial order $P = 4$.

3.3 CAD Reconstruction This section describes a novel method for reconstructing the lost CAD mesh connectivity which combines bottom-up approaches for vertex BRep association through the CAD API with a set of top-down logical operations derived from the B-Rep topology. This module is designed to mesh complex geometries and to be compatible with any linear mesh generator. To achieve this we have eliminated a large number of restrictions of the current processes. For example, it allows for lack of CAD conformity of the vertices and for the presence of multi-patches. Further, the new modules of NekMesh permit a full integration of third-party curved meshes. The final outcome of the process is the connectivity between the BRep and the mesh objects, as illustrated in Table 1 . Please note that we do not associate the mesh vertices with their BRep counterparts.

BRep and CAD-API All geometrical queries and operations are performed through one of two NekMesh CAD-APIs linked to the CAD engines of OpenCascade [5] and ITI CADfix [11]. OpenCascade has been

Table 1: Desired association between BRep and mesh objects.

CAD	Vertex	Edge	Face	EdgeNode	FaceNode
Node	(✓)	×	×	×	×
Curve	✓	✓	×	✓	×
Surf	✓	✓	✓	✓	✓

used in this study, but more details on the CAD-APIs can be found in references [25, 14].

The CAD-APIs read the BRep input data in STEP format. As the linear volume mesh is already generated, we can use the available mesh connectivity information to modify and relax the usually strict requirements on the STEP BRep of the current curving and CAD handling modules. The only requirement is a valid parametrisation of the CAD surfaces. This allows NekMesh to curve and optimise the linear mesh even in the presence of STEP artefacts like free edges, pierced surfaces, etc. that are hard to detect and fix in CAD repair.

Bottom-up BRep Preprocessing and Vertex Association The first step of the reconstruction process is to associate every boundary vertex of the linear mesh with the CAD surfaces. A naive approach that would query the distance to every BRep object is unfeasible for industrial geometries that may contain more than 10^4 surfaces. To reduce the cost of such queries, a preprocessing of the BRep is first performed. All CAD surfaces are sampled with nodes, extended and enclosed within bounding boxes which are stored in a k-D tree, as in the original NekMesh workflow [23].

This way every boundary vertex is efficiently associated with only a few candidate surfaces when it is inside their bounding box, see Figure 7. These can vary from 3 to 20 per vertex roughly depending on the CAD complexity. The vertex is then projected only onto the candidate surfaces, the surfaces are ordered according to the distance δ, and discard those where $\delta > \max(0.5L, 10^{-6})$ where L is the length of the edge. Finally we project the vertex to the closest CAD surface and reevaluate the list with the parametric location for all sufficiently close candidate surfaces.

This bottom-up approach gives approximate parametric locations of the mesh vertices for a list of CAD surfaces. We have adopted a top-down approach where the CAD information on the mesh vertices links the edges and faces to CAD surfaces because the use of bounding boxes creates a high degree of false associations in coarse regions and sliver surfaces leading to projections with distortions and tangled elements.

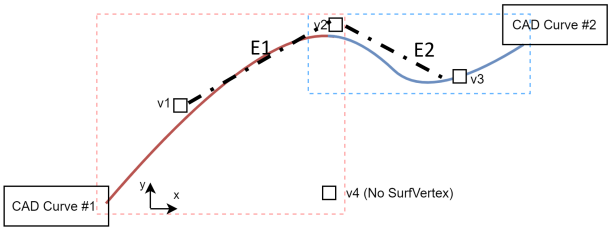

Figure 7: Diagram showing the process of vertex association to BRep objects before projection. Note that none of the vertices is exactly on the BRep. Vertices V_1 and V_3 will have only one associated BRep curve, whereas V_2 will have two.

Face-Associations The mesh vertices are now associated to their CAD surfaces, we now process the boundary faces. From a CAD-connectivity perspective, we consider three different types of elements: internal, corner, also referred to as (Case 2) elements, and multi-patch which span over two CAD surfaces (Case 3), as illustrated in Figure 8. We discuss the treatment of triangular boundary faces, but the method can be also be applied to quadrilateral faces. Their treatment is easier as they have fewer Case 2 elements.

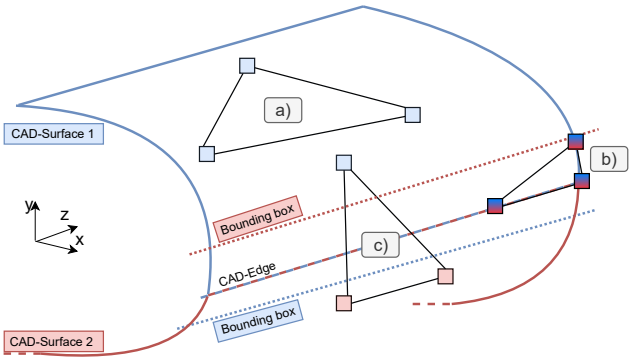

Figure 8: Diagram showing the 3 different element cases: (a) internal face, (b) corner (Case 2), and (c) multi-patch (Case 3).

The CAD reconstruction for "internal" elements is the easiest as all its vertices share a single common surface. In addition, at least one vertex is associated only with the common surface. These two conditions are usually met by more than 95% of the boundary elements and allow for better projection, and surface and volume optimisations by sliding elements and vertices on the surface.

Case 2 elements, with vertices having more than one common CAD surface, are more difficult to handle. These often appears when one of the surfaces is very

small or with a very high aspect ratio like, for example in blunt trailing edges or sliver surfaces as illustrated in Figure 9. In this case, the algorithm samples the mid-point on all edges and calculates the distance to the candidate CAD surfaces with the CAD API and then picks the one with the minimum overall deviation from the middle points. The surface ID is obtained as follows

$$\text{ID} = \arg\min_{k} \sum_{j=1}^{3} \|\mathbf{x}_j - \mathbf{P}_k(\mathbf{x}_j)\| \tag{3.1}$$

where $\mathbf{P}_k(\mathbf{x}_j)$ denotes the coordinates of the projection of the point $\mathbf{x}_j$ on the surface of ID k. This works well both for straight-sided and curved surfaces with reasonably high curvature deviation from the linear face.

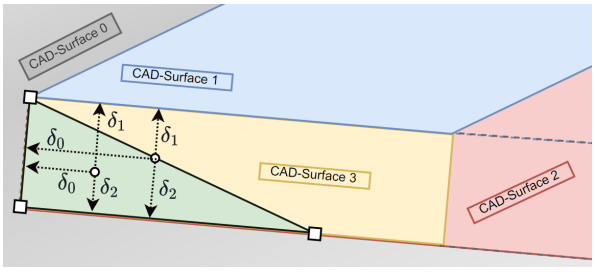

Figure 9: Specific treatment of the objects with multiple CAD surface candidates in a region of trailing edge or corner elements (Case 2).

Finally, if boundary face vertices do not share any common CAD surfaces or the element fails any of the previously described filters, no BRep object is associated to the element, Case 3 face. Hence, a simpler mesh curving algorithm is applied to this element without local surface optimisation and these face vertices do not slide on the CAD during the global volume optimisation.

Edge-association: The edge association to CAD surfaces is relatively straightforward. By revisiting Figure 7, it can be observed that when the vertices have a single associated common surface, this edge is internal to the BRep object and can directly be associated with it. A cross-check is performed with the parent elemental CAD surface.

If the vertices share two or more CAD surfaces, a more elaborate approach is required. Topologically, this indicates a corner edge likely generated on a CAD curve. Therefore, we loop over all curves, forming the EdgeLoops around the candidate CAD surfaces creating a shortlist of CAD curve candidates. If the edge has a single common one, it is connected to this CAD curve. If two curves are present (around junctions), another voting process is performed, choosing the closest one within a tolerance of 10^{-6}. In the case of more than two common CAD curves, we prefer the safer choice of assigning the elemental CAD surface to the edge to facilitate a more accurate projection and surface optimisation. Lastly, if the vertices of the edge do not share a CAD surface or fail the CAD curve tolerance test, this indicates that the edge is crossing multiple patches. Hence no BRep object is associated at this stage, and a simpler curving process is applied as per the Case 3 elements.

Extension to High-Order Meshes Once the mesh-CAD connectivity is available for the linear mesh, we can extend the method to high-order mesh entities such as edge nodes and face nodes. This is straightforward since the edge nodes will adopt the CAD curve or CAD surface of the parent edge, and the face nodes the CAD surface of the parent face. Interestingly, this brings about the unique workflow capability to restart the high-order meshing from any point of the process. Moreover, it allows to restart from any kind of a third-party mesh, being it linear or high-order .

3.4 Mesh Curving and Surface Quality

Once the connectivity between the linear mesh and the CAD-BRep is completed, we can apply any high-order mesh curving module. In this workflow, we modify and enhance the interpolative mesh curving algorithm, which is based on the parametric projection of high-order nodes onto the BRep. This has already been proven to produce high-quality meshes in the in-house bottom-up mesh generation workflow [25, 6]. However we can equally and successfully apply state-of-the-art algorithms such as variational optimisation [25] or approximate curving [20]. The parametric projection is applied hierarchically for every boundary face in the parametric space of the corresponding CAD surface parametric coordinates (u, v), hence, we first curve the edges and then the internal face nodes.

When we consider the edges, we first generate the high-order nodes in the reference space according to the user-defined order and quadrature rule, usually Gauss-Lobatto-Legendre. Then following the edge vertices in (u, v) parametric space, we can map the quadrature rule to the parametric space. Then from the parametric (u, v) coordinates of every high-order edge node, we use the CAD API to map back its location in Cartesian coordinates (x, y, z). The process is illustrated in Figure 10.

After the parametric projection of the edge nodes, we apply the same type of parametric projection on the

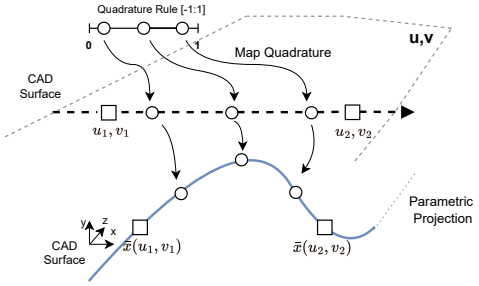

Figure 10: Diagram showing the projection of edge nodes from CAD surface parametric space (u, v) to Cartesian space (x, y, z).

corresponding internal face nodes, see Figure 11. Similarly, the desired quadrature nodes are generated according to the user-defined order and quadrature distribution, then mapped to the parametric space of the corresponding BRep surface with the parametric knowledge of the vertices. Last, these are projected on the CAD and the validity of the element is checked. This way, the workflow provides very high geometrical surface accuracy with the user-defined quadrature order, tested up to polynomial order $P = 14$.

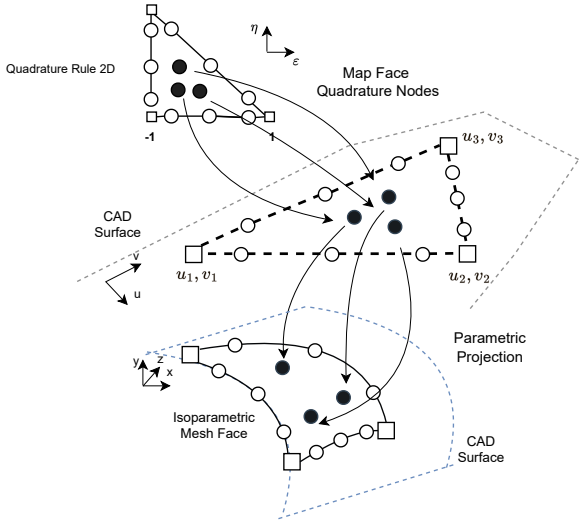

Figure 11: Diagram showing the 3D projection of the high-order face nodes in parametric (u,v) space for P4 mesh element.

In the rare cases where the boundary face does not have a CAD surface association, i.e. they are not CAD compliant, we rely on a simplified secondary mesh curving process. In this case, the face has at least one edge crossing two BRep objects. As discussed earlier, this is not a desirable situation where the exact parametric projection is not possible. However, when faced with BRep slivers or meshing from triangulation, it is crucial to account for them and devise strategies to avoid having linear or tangled elements. Therefore, we populate the desired quadrature on the linear element and then project the high-order edge nodes one by one to the closest CAD surface, as depicted in Figure 12. This fail-safe process relies on the curved edges to reconstruct the underlying geometry for robustness purposes. The reason being that projecting high-order face nodes on the closest CAD surface is more likely to result in self-intersections, especially when the two surfaces have high curvature and are only C_0 continuous. Moreover, no surface optimisation is applied to these mesh elements.

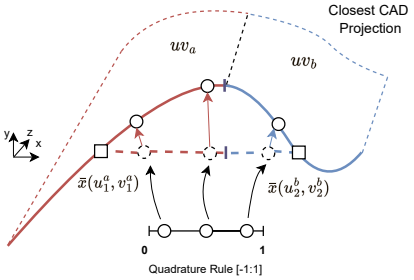

Figure 12: Diagram showing the 3D projection of edge nodes from Cartesian space (x, y, z) onto the closest CAD surface.

Surface Mesh Optimizations During the mesh curving, the workflow moves the high-order nodes on the BRep object to minimise the distortion induced by the parametric projection according to the optimization method described in references [21, 24]. On an edge, we achieve that by introducing a virtual spring network system between the edge nodes and moving them on the BRep object to minimise the potential energy

$$F = \sum_{i=1}^{P} \frac{||\mathbf{x}(u_{i+1}, v_{i+1}) - \mathbf{x}(u_i, v_i)||^2}{w_i}. \tag{3.2}$$

where the w_i are suitable weights for the chosen nodal distribution. A minimum of this energy is calculated in Cartesian space using a classical BFGS optimization algorithm [4]. This process becomes important when coarse elements are present in regions with very high two-directional curvature, such as wingtips or rounded trailing edges. In these cases, we observe a significant increase in the surface mesh quality, geometrical accuracy and even untangling of self-intersections, as shown in Figure 13. Naturally, this translates to an improved overall volume mesh quality.

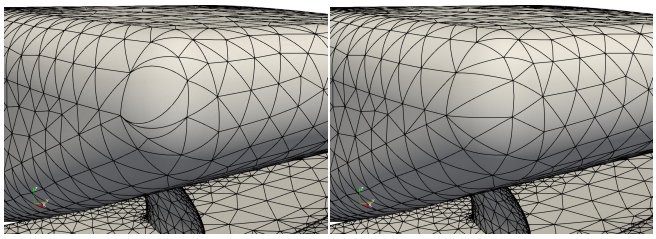

(a) (b)

Figure 13: The curved surface mesh generated with (b) and without(a) the optimisation. Note the presence of invalid elements when the optimisation is not applied.

3.5 Assessing Geometrical Mesh Accuracy through CAD-Reconstruction The geometrical errors in the mesh discretization of the underlying CAD could have a significant impact on the accuracy of simulations, especially for boundary layers at high flow speeds. Often it is difficult to identify these errors. The high-order extension of the CAD-Reconstruction algorithm provides a tool for assessing the geometrical accuracy of the mesh - the deviation from the target CAD-object $\delta\mathbf{x}$ and from the target CAD-Normal $\delta\mathbf{n}_i$.

The first stage of the process is to elevate (sample) the boundary face to an order of choice with the desired quadrature points on the face. Then the CAD connectivity is reconstructed and all vertices, high-order edges and face nodes receive their BRep parametric coordinates (u_i, v_i). This backward mapping allows us to then query through the CAD-API for the target location $\mathbf{x}_i$ and the unit normal vector $\mathbf{n}_i$ on the associated CAD object. Last, we calculate the corresponding nodal deviations for $\mathbf{x}_i$ and $\mathbf{n}_i$ between the isoparametric and BRep nodes, see Figure 14. Through the Nektar++ high-order utilities, we can visualise the elemental values of these deviations and assess if any further interventions are necessary. This also allows the user to visualise and investigate if, where and why an element does not have CAD associated with it which will indicate the presence of a multi-patch face or a rare failure of the CAD-Reconstruction algorithm.

3.6 Variational Optimizer The improvement of mesh quality and untangling of invalid element we (re)use the variational optimiser module in the NekMesh framework [24]. This is achieved through the minimisation of the deformation energy functional W, which is a function of the mapping ϕ from the ideal straight-sided element Ω_I^e to the curvilinear element Ω^e, formulated as find

$$\min_{\phi} \mathcal{E}_i(\nabla\phi) = \sum_{e\subset i} \int_{\Omega_I^e} W(\nabla\phi)\, d\mathbf{y}. \tag{3.3}$$

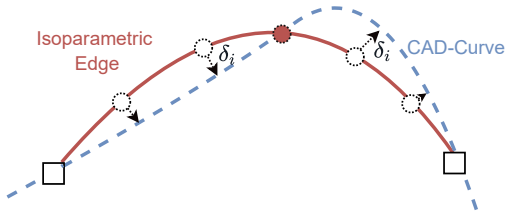

Figure 14: Diagram showing the mechanism of assessing the geometrical accuracy $\delta\mathbf{x_i}$ of a $P = 2$ mesh evaluated at $P = 6$ with an evenly distributed quadrature rule.

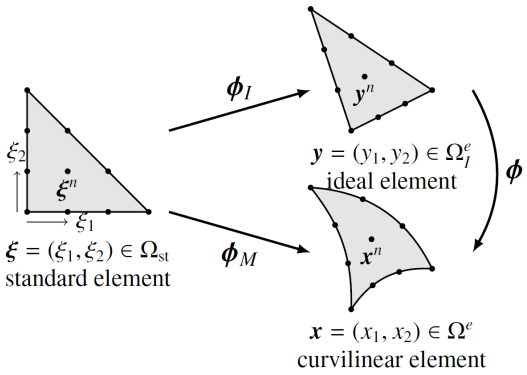

Figure 15: The mappings ϕ from standard reference element Ω_{st} to ideal straight-sided Ω_I^e and the final curved element Ω^e. Note that the mapping used for optimization is $\phi = \phi_M \circ \phi_I^{-1}$ [23].

The various mappings involved in this setting are depicted in Figure 15. The optimization calculates the positions of the nodes that lead to a minimum of the energy 3.3. We direct you to reference [25] for a detailed description of the method.

The energy functional adopted here is based on hyperelastic materials

$$W = \frac{\mu}{2}(\mathrm{Tr}(\mathbf{C}) - 3) - \mu \ln J + \frac{\lambda}{2}(\ln J)^2 \tag{3.4}$$

where $\nabla\phi(\mathbf{y})$ is the gradient tensor of the mapping, its determinant $J = \det(\nabla\phi)$ is denoted the Jacobian, λ and μ are the Lamé elastic constants, and $\mathbf{C}$ is the Cauchy-green stress tensor.

The untangling capability of the method is achieved through the regularisation of the Jacobian for values $J < 0$, and is significantly improved by allowing the movement of the nodes on the BRep object except for the mesh vertices associated with the CAD vertices. A minor limitation of our process is that we guarantee perfect CAD surface, but not perfect CAD curve and CAD vertex association. Therefore, for robustness, we also fix the nodes on the boundary associated with two or more surfaces, two or more curves and the ones

without a CAD object.

3.7 An Improved Isoparametric Boundary-layer Splitting Very high-aspect ratio elements are required near the boundary for viscous flow simulations. The main challenge is to propagate the curvature inside the domain and ensure the quality and validity of the final mesh. For this purpose, we employ the standard NekMesh approach for generating and curving a thick single prism layer around the body, the macro-prism layer [17]. Every macro-prism is mapped to standard space and it is split according to a user-defined progression ratio (r) and a number of boundary layers. This work introduces an improved implementation in NekMesh by propagating not only the edge curvature through the edge nodes but also all face nodes, hence providing higher surface accuracy.

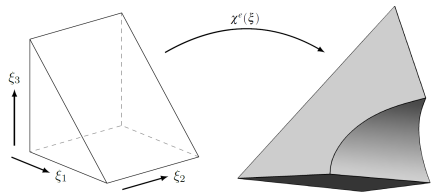

(a) Valid curved high-order macro-prism before splitting.

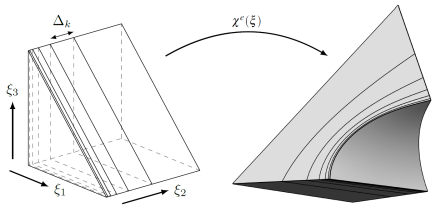

(b) Isoparametric splitting in reference space with $N = 6$ prism layers and a progression ratio $r = 1.5$.

Figure 16: Isoparametric boundary layer splitting in reference space (ξ) and the mappings from reference to Cartesian space [17].

4 Examples

We presnt two examples to illustrate the capabilities of the proposed approach: a simple domain surrounding a semi-sphere and an automotive geometry, the Imperial Front Wing [18, 3].

4.1 A Semi-spherical Geometry Test Case This elementary geometry represents a domain around a semi-sphere. The process works as follows: a very coarse linear mesh is generated from STEP in third-party software, consisting of only 4 prism elements representing the semi-sphere, see Figure 17a. The CAD-Reconstruction process successfully associated the necessary connectivity between all mesh elements and the BRep ones and performed purely parametric projections with surface optimisations to polynomial order $P = 7$, as described in Section 3, producing the mesh observed in Figure 17b. The achieved surface quality with a maximum geometrical deviation of $\delta = 1.3 \times 10^{-6}$ (tested with $P = 8$) shows that the proposed methodology is capable of reconstructing the geometry with very coarse meshes and very high-order polynomials, which is a unique capability of this implementation.

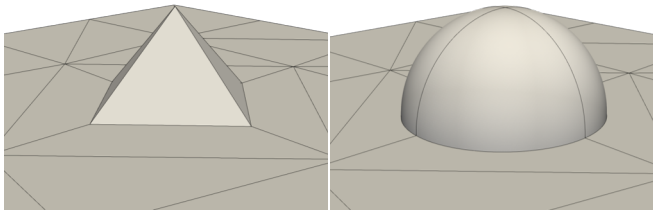

(a) (b)

Figure 17: The high-order mesh generation of a domain around semi-sphere starting from a linear mesh (a), the curved surface mesh with surface optimisation at polynomial order $P = 7$ (b).

Using the same geometry but with a finer all-tetrahedra linear mesh, we verify the consistency between the existing mesh generation workflow, as implemented by Turner [25], and the new proposed workflow. The linear mesh can be seen in Figure 18a. The process successfuly reconstructed all the CAD objects: 1650 vertices, 2474 edges, 1650 faces, and 6908 elements. This allowed the full utilisation of parametric mesh curving, surface optimisation and the variational optimiser with sliding of the internal to the CAD surfaces mesh nodes and vertices. As seen in the histogram of Figure 18c, the initial curved mesh is valid but with certain elements have low quality in terms of scaled Jacobian, with the minimum value of J_{min}=0.36. After the application of the variational optimiser, see Figure 18d, the overall quality of the mesh increases drastically, with a minimum scaled Jacobian of $J_{\min} = 0.865$. Both the geometrical accuracy and the final mesh quality are identical to the legacy internal bottom-up mesh generation workflow ($J_{\min} = 0.864$), which is a difference of less than 0.1%. This shows the consistency of the proposed methodology with the high-quality internal bottom-up one, which is to be expected due to the reuse of the high-order modules and the entirely successful CAD-Reconstruction.

4.2 Automotive Test Case: Imperial Front Wing This workflow aims at achieving a robust and automatic mesh generation for complex geometries. An

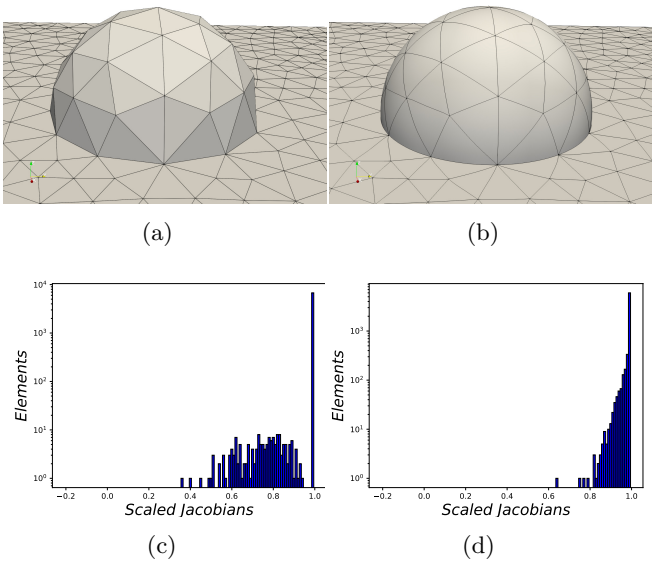

(a) (b) (c) (d)

Figure 18: The high-order mesh generation of a domain around a semi-sphere starting from a linear mesh (a), the curved surface mesh (b), the surface mesh after applying all optimisation processes (c), and a histogram showing the final quality of the mesh (d).

essential part of such geometry and focus from a design perspective is the front wing of a motorsport car and, hence, the choice for this demonstration.

The Imperial Front Wing, is an open geometry from a F1 car provided by McLaren Racing [3]. The front wing, shown in Figure 19, consists of a mainplane, two wing flaps, a nose cone, a Gurney flap, a canard, a side endplate with a connected footplate. The STEP BRep of the domain consisted of 351 vertices, 559 curves and 209 surfaces. It has a minimum edge length of 4×10^{-4}m, a maximum plane length of 0.2m, and a minimum radius of curvature of 2×10^{-4}m. Note the very small radius of curvature and large ratio of maximum to minimum lengths.

First, a linear straight-sided mesh is generated directly from the STEP BRep in the third-party finite volume mesh generator, StarCCM+, see Figure 20. No CAD defeaturing or simplifications are applied, and CAD compliance is imposed on the whole geometry to demonstrate the reconstruction algorithm. The only region where this is not enforced is the footplate leading edge to avoid sliver elements, see Figure 5. A single thick prism layer is generated near the body, which is sufficiently thick to accommodate the mesh curving process, and a tetrahedral mesher is used internally inside the domain. The resulting mesh can be seen in Figure 20 and some information about the mesh-entities in Table 2.

Once converted to NekMesh format, the CAD-Reconstruction algorithm is applied successfully as it can be seen in Table 2. Due to the application of bounding boxes extending the surfaces, it was capable of associating all vertices to at least one BRep surface even if vertex deviation was initally present with a deviation $\delta = 3 \times 10^{-6}$ from the BRep. The only exceptions are 5 elements located at the end-plate region where the CAD conformity was deliberately not enforced, leading to multi-patch linear elements. These 5 elements amount for for less than 0.01% of the prism elements on the boundary. The module did not associate CAD objects to 34 edges, representing 0.04% of the surface edges. Note that the discrepancy between elements without CAD object and edges without CAD objects is expected due to the retrofitting nature of the process and the independent queries of edges and elements that include tolerances.

Table 2: Statistics on CAD-Reconstruction module. Vertices, Edges and Faces are only counted on the IFW.

Mesh Bnd Obj.	Overall	No-CAD/$J < 0$	Fail[%]
Vertices	27 839	0	0%
Edges	83 339	34	0.04%
Faces	55 499	5	0.01%
Elements Tets	398 548	0	0%
Elements Prism	56 592	0	0%

The most critical step for these geometries is the mesh curving one to the desired polynomial order, in this case, p=5 with Gauss-Lobatto-Legendre points. As there are also elements and edges without CAD object, the curving module first uses the fail-safe simplified projection on these 34 edges and isolates them from the optimisation processes. For the rest of the boundary edges and elements, we can use the more accurate parametric projection and the surface optimisation presented in Section 3.4. This leads to a highly smooth isoparametric surface, see Figure 21, even for coarse mesh resolution in regions with high non-uniform curvatures.

As expected, the smooth isoparametric surface from Figure 21 results in high geometrical accuracy once it is estimated. The vertices are ensured to be CAD-conforming and lie within a distance $\delta \approx 10^{-10}$, hence within the CAD-API tolerance. The deviation from the CAD is $\delta = 6.4 \times 10^{-7}$ when tested with $P = 6$ evenly spaced points. The maximum values appear in the regions with the highest non-uniform curvatures and coarsest resolution, with leading edges reconstructed by just two or three faces, and around the simplified projections, see Figure 22. The module indicates some higher values around the symmetry plane, but after observation, these were found to be artefacts of the secondary run of face-nodes associations and not real

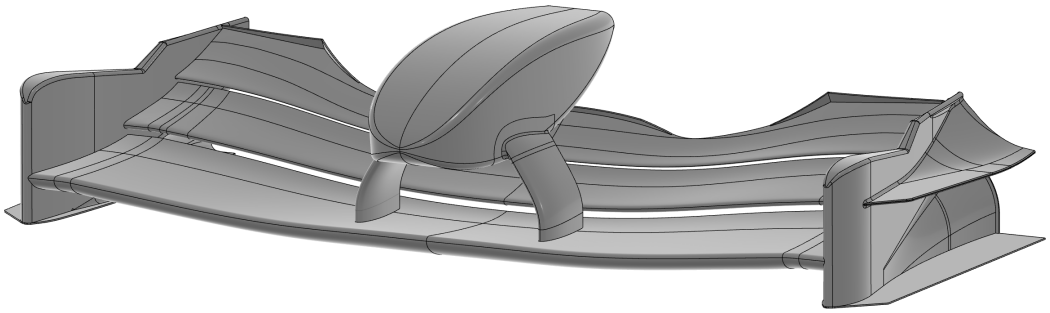

Figure 19: The CAD BRep geometry of the Imperial Front Wing (IFW).

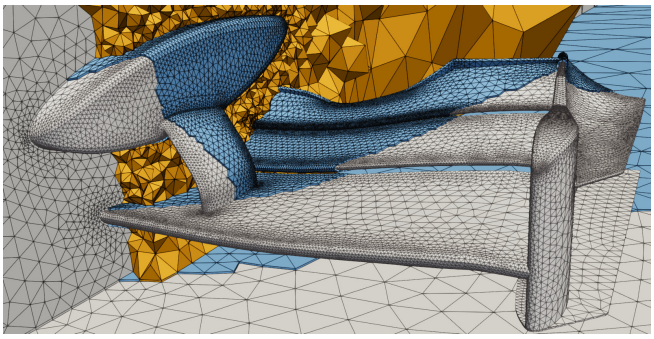

Figure 20: A linear mesh of the Imperial Front Wing. The surface mesh is coloured in grey, the prism layers in blue and the tetrahedra in yellow.

surface discrepancies. Depending on the applications and the Reynolds Number, the user might use this information and assess if mesh resolution or polynomial order should be increased.

It is also possible to apply the variational optimiser to try to improve the mesh quality. We limit the optimisation to regions with $J < 0.6$ for computational efficiency. Initially, the mesh is invalid and has five elements with negative Jacobians. The quality after the application of the optimiser can be seen in Figure 23. The histogram does not show as impressive quality as the semi-sphere, but this can be explained by two factors. First that the initial mesh is very distorted and second that only limited CAD sliding was allowed in the process due to the very thin CAD surfaces in the geometry. This also points out the potential of CAD-sliding between BRep objects.

Finally, following the generation of the isoparametric boundary layer for ensuring a suitable mesh resolution for the required local distance y^+, this workflow provides the high-order meshes that are currently employed for incompressible flow simulations. With similar meshes for the Imperial Front Wing being currently run in the Nektar++ group as part of the SSeCOID project, see Figure 24 for the current simulation status. It shows

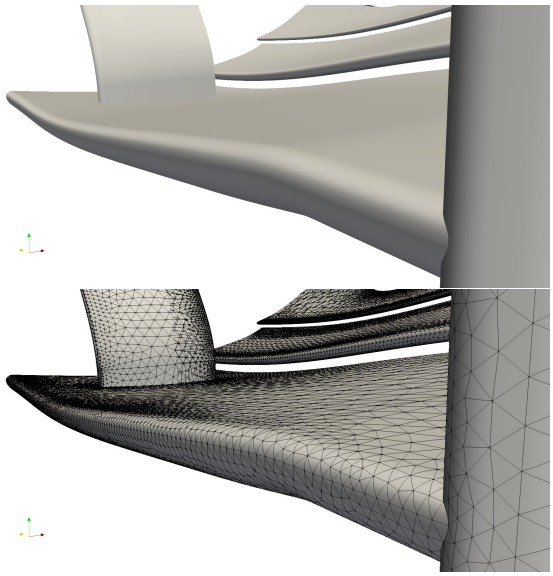

Figure 21: Surface quality shown for an enlargement of the isoparametric surface mesh.

the pressure field calculated using the Nektar++ incompressible iLES flow solver after 1.2CTU[1] starting from an initial RANS solution.

5 Current Work

Ongoing work is applying the pipeline to generate a high-order mesh for a full F1 car geometry with more than 9 000 CAD surfaces. Preliminary results indicate that the workflow scales and can achieve good surface accuracy with a full prismatic layer around the car, without defeaturing the CAD geometry. However, it has also highlighted some areas of improvement.

Extending Mesh Modification Techniques to 3D
The main limitation of the workflow is the assumption

[1]Convective time units: time it takes the flow to traverse a domain length.

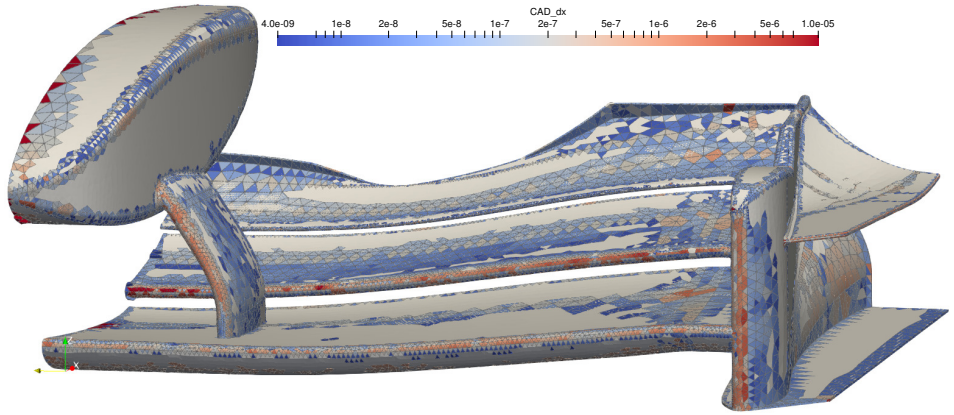

Figure 22: The maximum elemental geometrical deviation from the BRep of the isoparametric mesh as evaluated at evenly spaced intervals with $P = 6$. Only surface elements with $\delta > 10^{-9}$ are visualised.

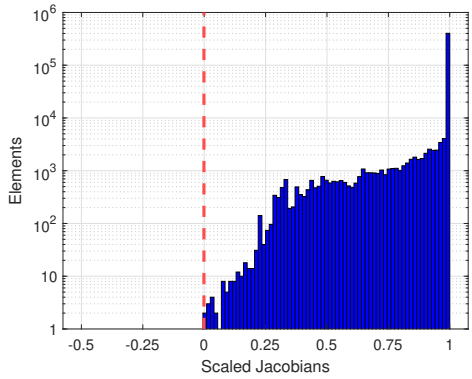

Figure 23: Histogram of the distribution of scaled Jacobians in a high-order IFW mesh with $P = 5$ at the end of the meshing workflow.

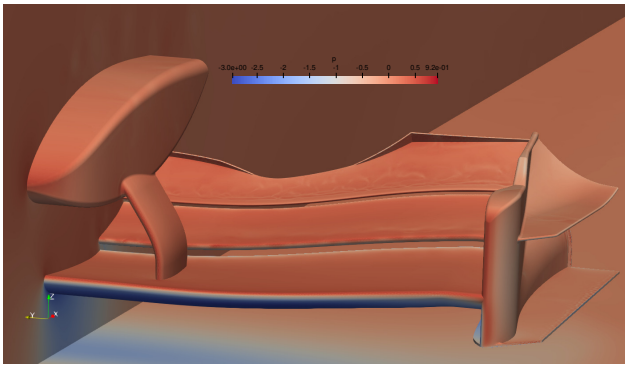

Figure 24: Early Nektar++ simulation of the pressure field around the IFW at $t = 1.2$CTU (0.25s), initialized from a RANS field.

that the linear straight-sided mesh is ideal. Hence, we are extending our work on 2D isoparametric mesh modification techniques [13] to 3D with the goal of optimising the overall mesh quality of the mesh generator. These include isoparametric splitting and coarsening, face swap and edge collapse for hybrid meshes of prisms and tetrahedra.

Variable Isoparametric Prism Layer Splitting Currently, the module uses the same settings over the whole O-type boundary layers of a body. When complex geometries with proximities or blunt trailing edges are meshed, these regions become a limiting region for the CFL. Therefore, an alleviation of the problem is the use of a progression ratio $r = 1.0$ or collapsing a prism layer before reaching this region while keeping the user-defined ratio r in the rest.

6 Conclusions

We have presented and discussed a new improved workflow for high-order mesh generation from third-party meshes focusing on the CAD-Reconstruction process, its advantages and the potential risks when using third-party meshes. A new method for reconstructing BRep parametrisation of mesh entities allows us to fully merge third-party linear mesh generators, or even high-order meshes, with modern high-order methods. Its implementation also provides a suitable metric for assessing the geometrical accuracy of high-order meshes with reference to a given CAD BRep. Finally, we demonstrated some of the capabilities of the proposed workflow for both simple academic and complex industrial automotive geometries.

Acknowledgements

This project has received funding from the European Union's Horizon 2020 research and innovation programme under the Marie Skłodowska-Curie grant agreement No. 955923. The authors greatly appreciate the contribution of Alexandra Liosi who produced the solution snapshot for the simulation of the Imperial Front Wing shown here.

References

[1] OpenFOAM, API guide: `ccmToFoam.C` file reference. `https://www.openfoam.com/documentation/guides/latest/api/ccmToFoam_8C.html`. Last accessed October 2023.

[2] *PADRAM: Parametric Design and Rapid Meshing System for Complex Turbomachinery Configurations*, volume Volume 8: Turbomachinery, Parts A, B, and C of *Turbo Expo: Power for Land, Sea, and Air*, 06 2012.

[3] F.F. Buscariolo, J. Hoessler, D. Moxey, A. Jassim, K. Gouder, J. Basley, Y. Murai, G.R.S. Assi, and S.J. Sherwin. Spectral/hp element simulation of flow past a formula one front wing: Validation against experiments. *Journal of Wind Engineering and Industrial Aerodynamics*, 221:104832, 2022.

[4] R.H. Byrd, P. Lu, J. Nocedal, and C. Zhu. A limited memory algorithm for bound constrained optimisation. *SIAM Journal on Scientific Computing*, 16(5):1190–1208, 1995.

[5] Capgemini Engineering. Open Cascade, Last accessed January 2023.

[6] S. Chun, J. Marcon, J. Peiró, and S.J. Sherwin. Reducing errors caused by geometrical inaccuracy to solve partial differential equations with moving frames on curvilinear domain. *Computer Methods in Applied Mechanics and Engineering*, 398:115261, 2022.

[7] P.F. Fischer, J.W. Lottes, and S.G. Kerkemeier. nek5000 Web page, 2008. http://nek5000.mcs.anl.gov.

[8] T. Gerhold and J. Neumann. The parallel mesh deformation of the DLR TAU-code. In C. Tropea et al., editor, *New Results in Numerical and Experimental Fluid Mechanics VI*, pages 162–169. Springer Berlin Heidelberg, 2008.

[9] C. Geuzaine and J.-F. Remacle. Gmsh: A 3-D finite element mesh generator with built-in pre- and post-processing facilities. *International Journal for Numerical Methods in Engineering*, 79(11):1309–1331, September 2009.

[10] M.D. Green, K.S. Kirilov, M. Turner, J. Marcon, J. Eichstädt, E. Laughton, C.D. Cantwell, S.J. Sherwin, J. Peiro, and D. Moxey. Nekmesh: An open-source high-order mesh generation framework. *Computer Physics Communications (preprint)*, 2024.

[11] ITI-Global. CADfix: CAD translation, healing, repair, and transformation. 2017.

[12] S.L. Karman, K. Karman-Shoemake, and C.D. Woeber. Mixed order mesh curving. *SEMA SIMAI Springer Series*, 30:1–21, 2022.

[13] K. Kirilov, A. Sanderson, and M. Kirby. Pre-/post-processing & performance session. 2023. Nektar++ Workshop 2023.

[14] J. Marcon, M. Turner, J. Peiró, D. Moxey, C. R. Pollard, H. Bucklow, and M. Gammon. High-order curvilinear hybrid mesh generation for CFD simulations. In *2018 AIAA Aerospace Sciences Meeting*, 2018.

[15] G. Mengaldo, D. Moxey, M. Turner, R.C. Moura, A. Jassim, M. Taylor, J. Peiró, and S.J. Sherwin. Industry-relevant implicit large-eddy simulation of a high-performance road car via spectral/*hp* element methods. *SIAM Review*, 63(4):723–755, 2021.

[16] D. Moxey, C.D. Cantwell, Y. Bao, A. Cassinelli, G. Castiglioni, S. Chun, E. Juda, E. Kazemi, K. Lackhove, J. Marcon, G. Mengaldo, D. Serson, M. Turner, H. Xu, J. Peiró, R.M. Kirby, and S.J. Sherwin. Nektar++: Enhancing the capability and application of high-fidelity spectral/*hp* element methods. *Computer Physics Communications*, page 107110, 2019.

[17] D. Moxey, M.D. Green, S.J. Sherwin, and J. Peiró. An isoparametric approach to high-order curvilinear boundary-layer meshing. *Computer Methods in Applied Mechanics and Engineering*, 283:636–650, 2015.

[18] J.M. Pegrum. *Experimental study of the vortex system generated by a Formula 1 front wing.* PhD thesis, Imperial College London, 2007.

[19] E. Ruiz-Gironés and X. Roca. Generation of curved meshes for the high-lift common research model. *CoRR*, abs/2211.08183, 2022.

[20] E. Ruiz-Gironés, X. Roca, and J. Sarrate. High-order mesh curving by distortion minimization with boundary nodes free to slide on a 3D CAD representation. *Computer Aided Design*, 72:52–64, 2016.

[21] S.J. Sherwin and J. Peiró. Mesh generation in curvilinear domains using high-order elements. *International Journal for Numerical Methods in Engineering*, 53(1):207–223, 2002.

[22] T. Toulorge, C. Geuzaine, J.-F. Remacle, and J. Lambrechts. Robust untangling of curvilinear meshes. *Journal of Computational Physics*, 254:8–26, 2013.

[23] M. Turner, D. Moxey, and J. Peiró. Automatic mesh sizing specification of complex three dimensional domains using an octree structure. In *24th International Meshing Roundtable*, 2015.

[24] M. Turner, D. Moxey, J. Peiró, M. Gammon, C.R. Pollard, and H. Bucklow. A framework for the generation of high-order curvilinear hybrid meshes for CFD simulations. In *Procedia Engineering*, volume 203, pages 206–218, 2017.

[25] M. Turner, J. Peiró, and D. Moxey. Curvilinear mesh generation using a variational framework. *Computer-Aided Design*, 103:73–91, 2018.

[26] F.D. Witherden, A.M. Farrington, and P.E. Vincent. PyFR: An open source framework for solving advection–diffusion type problems on streaming architectures using the flux reconstruction approach. *Computer Physics Communications*, 185(11):3028–3040, 2014.